

Weighing in on the Seismic Scale: The use of Seismic Fault Measurements for Constructing Discrete Fracture Networks in the Horn River Basin

Carl A. Reine*

Nexen Inc., Calgary AB, Canada

carl_reine@nexeninc.com

and

Rory B. Dunphy

Nexen Inc., Calgary AB, Canada

Summary

Discrete Fracture Network (DFN) models (Rogers et al., 2010) are a useful tool to understand and quantify the impact of natural fracture networks on hydraulic fractures. In our Horn River basin example, we use a multi-scale approach to derive key input distributions to the DFN such as length, azimuth, and fracture intensity. We augment small-scale fracture measurements from core and image log data with large-scale measurements from outcrop and 3D seismic. The use of seismic data in particular adds a critical scale of measurement to the data, allowing the formation of more robust distributions. Furthermore, a seismically derived fault intensity map may be used to scale the spatial variability of the DFN model.

Introduction

A common concept in shale gas plays is the notion of generating fracture complexity, or a wide fracture fairway, during hydraulic stimulation (Fisher et al., 2004). This has implications for proppant placement, fracture conductivity, and ultimately the production profile of a well (Cipolla et al., 2008). Evidence from the Barnett shale suggests natural fractures exert a fundamental control on this process (Gale et al., 2007).

A DFN model is a means of constructing a realistic natural fracture network using statistical descriptions of the input parameters (Dershowitz et al., 2010). Key inputs for the model include distributions of fracture length, azimuth, intensity, aperture, and transmissivity. The last two parameters are driven primarily by image log measurements and well tests, and it is with the remaining three that multiple scales of data become most useful. With a completed DFN model, hydraulic fractures may be simulated such that they account for appropriate interactions with the natural system (Figure 1).

Method

To determine the distribution of fracture length, we exploit the fact that it commonly obeys a power-law distribution (Bonnet et al., 2001) (Figure 2). At small scales, measurements of fracture length may be determined from core and image log data, extending to meso-scales using outcrop measurements (Figure 3). Single-scale measurements require an extrapolation of the distribution to the scale of interest for the model, typically 5 m - 200 m. However, limitations in the measurements restrict the ability to make this extrapolation from small ranges of scale. Deviations from the distribution trend are caused by ‘censoring’, when poor sampling occurs as a result of fractures and the sampled region being at the same scale, or by ‘truncation’, when the size of fractures is below the resolution of the measurements (Bonnet et al., 2001).

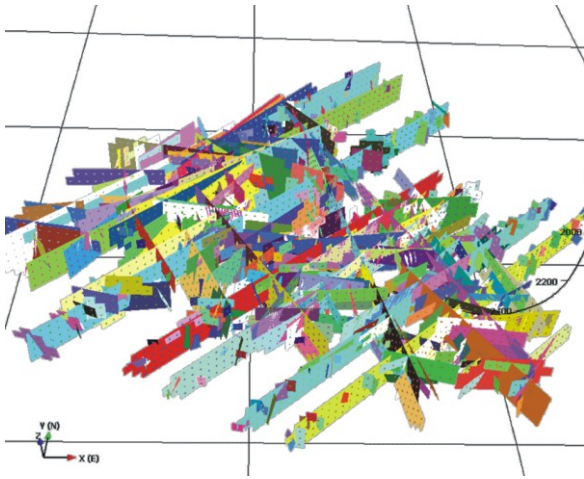


Figure 1. An example of a simulated hydraulic fracture process using a realization of the statistically defined DFN model. Coloured planes correspond to failed fractures.

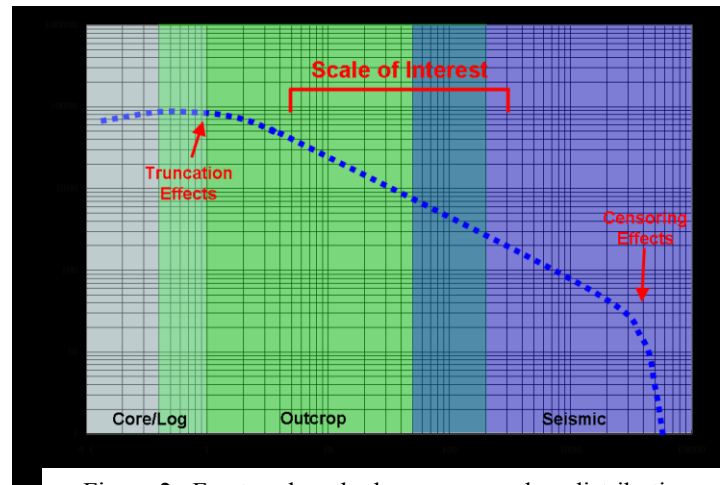


Figure 2. Fracture length obeys a power-law distribution. Small-scale observations using core and image logs require extrapolation to the scale of interest. Censoring and truncation effects must also be considered.

While many fractures that are key to reservoir production are below the resolution of seismic data, the power-law relationship allows us to exploit the large spatial coverage of 3D to include larger and more sparsely populated faults in the reservoir measurements, improving the statistical validity of the distribution.

To maximize our ability to identify faults on the seismic data, we make use of seismic coherence (Bahorich & Farmer, 1995), which provides a means of highlighting discontinuities in reflections. To enhance these discontinuities even more, we also interpret faults on data which has been filtered with a narrow band-pass filter (Hesthammer, 1999; Sun et al., 2010). Figure 4 shows the original seismic data, as well as data which has been spectrally decomposed around 30 Hz. The coherence volumes from these two seismic classes are also shown, and it is evident that the 30 Hz data is a valuable tool for identifying discontinuities. Faults are picked on the data, and the intersections with reservoir horizons are traced laterally.

The second set of seismic information that is available comes from inferred discontinuities, as measured by seismic curvature attributes (Roberts, 2001). These attributes highlight structures that are just below the resolution of seismic imaging, but whose existence may be inferred by structural deformation (Murray, 1968; Chopra & Marfurt, 2007). We extract maps of curvature attributes at the reservoir level, and trace lineaments which fall above a certain amplitude threshold.

Using the two sets of seismic information: the directly observed discontinuities and the inferred discontinuities, we perform a statistical analysis of the fault lengths and azimuths. The lateral traces of the discontinuities are first modelled in a least-squares fashion as linear events. The points of the traces are then projected back onto the linear model, which allows for the length and azimuth to be calculated.

The azimuth distribution for over 200 seismic lineaments is shown in Figure 5, along with the fracture azimuth distribution determined from image logs. Both distributions have a maximum population of azimuths centered around 37.5° . The seismic data however, has a greater prevalence of events in the North-South direction. Because the inferred seismic discontinuities rely on the assumption that structure indicates faulting, not all of these events are necessarily useful in our analysis. It is thus possible to filter the inferred seismic events based on the azimuth distribution obtained from the image logs. These filtered seismic events are then used to populate the large-scale end of the length distribution.

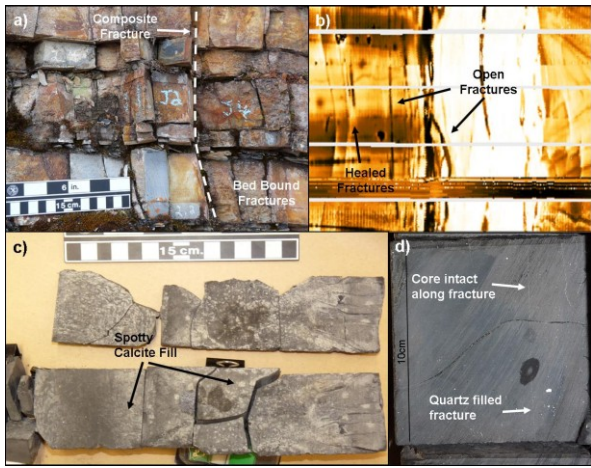


Figure 3. Small-scale examples of fracture information. a) Northeast BC Devonian shale outcrop showing multiple fracture sets. b) Image log data in a horizontal well through the Muskwa/Otter Park formation. Core data showing c) partially open and d) closed fractures in the Muskwa/Otter Park formation.

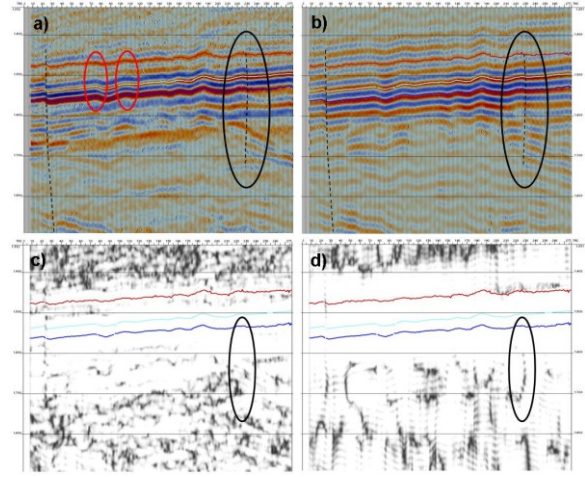


Figure 4. a) Original seismic data. Two faults are identified by dashed lines, and examples of two curvature features are circled in red. b) The 30 Hz data more clearly highlights the discontinuities in the events, allowing some faults (circled) to be more easily identified. The coherence volumes for a) and b) are shown in c) and d) respectively.

Finally, we define a 2D grid over our area of interest for the purpose of calculating a fault intensity map, derived in a similar fashion to Easley et. al (2010). The fault intensity map is defined by the cumulative length of all lineaments in a grid cell, divided by the grid cell area (Figure 6) (Dunphy, 2003). Although this intensity measurement is only for the large-scale fractures, it can then be used to scale measurements from image logs to develop a spatially-variant fracture intensity. This property can then be input to the DFN model for characterizing the field. The grid-based approach also allows us to map other fracture properties, such as length-weighted average azimuth, and similarity to expected azimuth.

Conclusions

Single-scale measurements of fractures leads to misrepresentations of natural systems due to the spatial and resolution limitations of the measurement technique. By combining fracture measurements at the core, image log, outcrop, and seismic scales, we achieve a more robust representation of the natural fracture system. Furthermore, by making use of the large areal coverage of the 3D seismic, we are able to develop a spatially-variant DFN model to characterize our field.

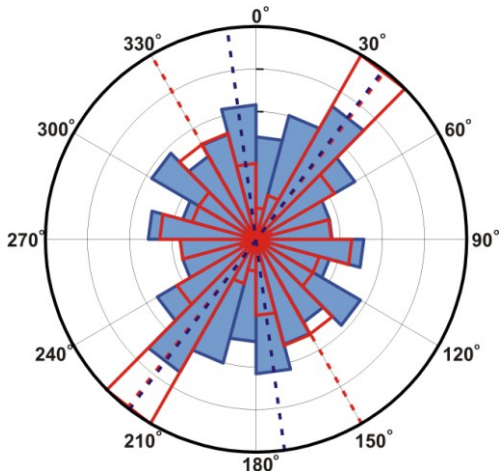
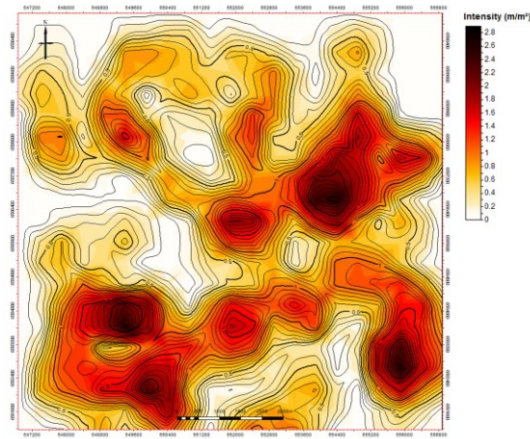


Figure 5. Azimuthal distribution of fracture measurements from image log data (red) and seismic data (blue filled). A maximum population occurs at 37.5° for both seismic and log measurements, and a secondary population is seen at -30° for the log data and -7.5° for the seismic data. The seismic data shows a more isotropic response, suggesting that not all of the inferred faults are actually significant.

Figure 6. Seismically defined fault intensity map. The fault intensity is a gridded measurement of cumulative fault length per unit area. These measurements of high- (dark red) and low-intensity (white) regions may be used to drive the spatial variations in the DFN model.



References

- Bahorich, M., and S. Farmer, 1995, 3D Seismic Discontinuity For Faults And Stratigraphic Features: The Coherence Cube: The Leading Edge, **14**, 1053-1058.
- Bonnet, E., O. Bour, N.E. Olding, P. Davy, I. Main, P. Cowie, and B. Berkowitz, 2001, Scaling Of Fracture Systems In Geological Media: Reviews of Geophysics, **39**, 347-383.
- Chopra, S., and K. Marfurt, 2007, Curvature Attribute Applications To 3D Surface Seismic Data: The Leading Edge, **26**, 404-414.
- Cipolla, C.L., N.R. Warpinski, M.J. Mayerhofer, E.P. Lolon, and M.C. Vincent, 2008, The Relationship Between Fracture Complexity, Reservoir Properties, And Fracture Treatment Design: Annual Technical Conference and Exhibition, SPE, Expanded Abstracts, 115769.
- Dershowitz, W.S., M.G. Cottrell, D.H. Lim, T.W. Doe, A Discrete Fracture Network Approach For Evaluation Of Hydraulic Fracture Stimulation Of Naturally Fractured Reservoirs: 44th US Rock Mechanics Symposium, ARMA, Expanded Abstracts, 10-475.
- Dunphy, R.B., 2003, The Role Of Fracture Systems In Controlling Groundwater Yields In The Post-Silurian Rocks Of Ireland: M.Sc. thesis, University of Dublin, Trinity College.
- Easley, D., F. Yustiana, A. Hidayat, 2010, Seismic Lineament Analysis Of A Fractured Limestone Reservoir In The Ujung Pangkah Field: 80th Annual Meeting, SEG, Expanded Abstracts, 1347-1351.
- Fisher, M.K., J.R. Heinze, C.D. Harris, B.M. Davidson, C.A. Wright, and K.P. Dunn, 2004, Optimizing Horizontal Completion Techniques In The Barnett Shale Using Microseismic Fracture Mapping: Annual Technical Conference and Exhibition, SPE, Expanded Abstracts, 90051.
- Gale, J.F.W., R.M. Reed, and J. Holder, 2007, Natural Fractures In The Barnett Shale And Their Importance For Hydraulic Fracture Treatments: AAPG Bulletin, **91**, 603-622.
- Hesthammer, J., 1999, Improving Seismic Data For Detailed Structural Interpretation: The Leading Edge, **18**, 226-247.
- Murray, G.H., 1968, Quantitative Fracture Study - Spanish Pool, McKenzie County, North Dakota: AAPG Bulletin, **52**, 57-65.
- Roberts, A., 2001, Curvature Attributes And Their Application To 3D Interpreted Horizons: First Break, **19**, 85-100.
- Rogers, S., D. Elmo, R. Dunphy, and D. Bearinger, 2010, Understanding Hydraulic Fracture Geometry And Interactions In The Horn River Basin Through DFN And Numerical Modeling: Canadian Unconventional Resources & International Petroleum Conference, CSUG/SPE, Expanded Abstracts, 137488.
- Sun D., Ling Y., Guo X., Gao J., and Lin J., 2010, Application Of Discrete Frequency Coherence Cubes In The Fracture Detection Of Volcanic Rocks In Full-Azimuth Seismic Data: 80th Annual Meeting, SEG, Expanded Abstracts, 1342-1346.